Dynamics of the Dissociating Uracil Anion Following Resonant Electron Attachment

Y. Kawarai,[†,‡] Th. Weber,[‡] Y. Azuma,[†] C. Winstead,[¶] V. McKoy,[¶]
A. Belkacem,[‡] and D.S. Slaughter[*,‡]

Department of Materials and Life Sciences, Sophia University, Japan, Chemical Sciences Division, Lawrence Berkeley National Laboratory, Berkeley, USA, and California Institute of Technology, Pasadena, USA

E-mail: DSSlaughter@lbl.gov

[*]To whom correspondence should be addressed
[†]Department of Materials and Life Sciences, Sophia University
[‡]Chemical Sciences Division, Lawrence Berkeley National Laboratory
[¶]California Institute of Technology

Abstract

We report a combined experimental and theoretical investigation of dissociative electron attachment (DEA) to the nucleobase uracil. Using ion momentum imaging experiments employing a DEA reaction microscope we have measured 3-dimensional momentum distributions of specific anionic fragments following DEA to uracil by 6 eV electrons. From the measured anion fragment kinetic energy we determine the possible dissociation pathways and the total kinetic energy release. We employ electronic structure and electron scattering calculations to determine the probability for electron attachment in the molecular frame. Combining these calculations with the imaging measurements we reveal several key features of the coupled electronic and nuclear dynamics of DEA.

Graphical TOC Entry

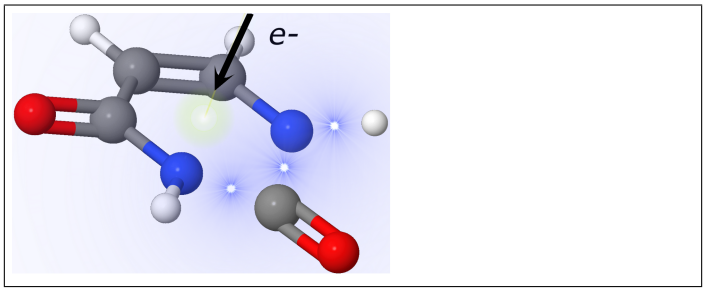

Keywords

transient anion,electron attachment,anion dynamics,resonant dissociation,DEA,electron impact excitation

A unique capability of low-energy free electrons is to cleave specific molecular bonds through resonant processes. These processes include excitation and electron attachment to dissociative intermediate states. Dissociative electron attachment (DEA) is mediated by transient anion states that are ubiquitous in low-energy electron-molecule collisions for incident electron energies both above and below the first electronic excitation threshold. In bulk matter secondary electrons are produced in high abundance by primary ionizing radiation, on the order of a few 10^4 low-energy electrons per MeV of deposited energy.[1–3] These secondary electrons likely play a decisive role in DNA strand breaks and the volume over which damage occurs around the primary irradiation sites.[1]

One important characteristic of DEA is that specific bonds may be targeted for dissociation by Nature or the experimentalist as a function the incident electron energy. The internal motion before and during the dissociation of the transient anion that is formed upon electron attachment dictates the fragmentation and non-dissociative relaxation mechanisms that protect biomolecules from damage by ionizing radiation. Despite the importance of understanding these phenomena in biological systems, little is known about the dynamics of DEA in biologically relevant molecules. For gaseous systems, experimental techniques have recently advanced to enable measurement of the non-Born-Oppenheimer dynamics of polyatomic transient anions[4–11] by momentum imaging of the dissociation products.

The RNA nucleobase uracil (U) contains many of the functional groups common to the DNA bases, while being more tractable for gas-phase experiments due to its relatively high vapor pressure and its single tautomer in the ground state.[12] Denifl and co-workers[13] reported 13 DEA fragmentation channels from uracil vapor in the 0-14 eV region by experiments employing high-resolution mass spectrometry. The site-selectivity for H^- production from uracil and thymine (5-methyluracil) anions was investigated as a function of incident electron energy by Ptasińska *et al.*[14] using electron-molecule crossed-beams experiments and recently by Almeida *et al.*,[15] with electron transfer from atom-molecule collision experiments. In another recent study, Ferreira da Silva *et al.*[16] reported that the abundant NCO^- fragment

that occurs above 4 eV electron attachment energy in DEA to uracil and thymine results predominantly from a sequential process: the relatively fast decay of the uracil transient anion by ejection of neutral hydrogen proceeds and is followed by a slower unimolecular decomposition of the remaining anion. By substituting methyl groups at the nitrogen sites in thymine they determined that the remarkable bond-specificity as a function of resonant electron energy in the first step is conserved through to the second slower and more complex reaction.

In the present experiments we tuned the incident electron energy to the 6 eV resonance reported in the DEA ion yield spectra of Denifl *et al.*[13] that is near the low-energy onset of several ring-breaking fragmentation channels. Momentum images were recorded for the 6 major fragmentation channels at this energy, with relative ion yields for each fragment found to be in good agreement with the data of Denifl *et al.*[13] We first categorize the DEA fragmentation channels that yield a fragment anion with peak kinetic energy less than 0.1 eV, i.e. ions having thermal kinetic energy within the resolution of the experiment. Fig. 1 illustrates the momentum and kinetic energy distributions of the ions produced in each of these fragmentation channels.

We determine the energy difference between the initial and final electronic states of the DEA reaction by the relation $\Delta E = \Sigma_i D_i - EA$, where D_i are the relevant bond dissociation energies of the transient anion and EA is the adiabatic electron affinity of the parent of the anionic fragment. Since the lowest two bond dissociation energies for uracil breakup are expected to be 4.4 and 5.0 eV,[13,17] we do not expect DEA at 6 eV to produce more than two fragments unless the vertical electron affinity of the anion parent is higher than $\sim$ 3.4 eV. The adiabatic electron affinities of CN, NCO and the uracil-yl [U $-$ H] family of radicals are 3.9 eV, 3.6 eV and 2.35 - 3.8 eV, respectively,[17–19] therefore it is possible that DEA in the 5 - 11 eV electron energy range leads to multiple fragments in each of the channels of Fig. 1. The kinetic energy spectra of Fig. 1(e) are likely due to three-body dissociation, with significant vibrational excitation of the molecular fragments and little kinetic energy transferred to

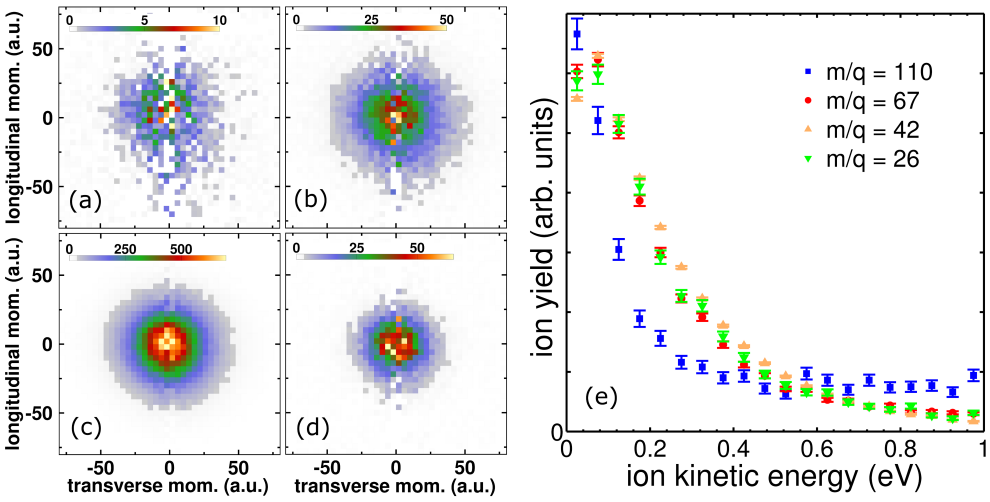

Figure 1: Measured ion momentum distribution following DEA to uracil at 6.0 eV electron energy (a) 110 atomic mass units (amu), $C_4H_2N_2O_2^-$, (b) 67 amu, C_3HNO^-, (c) 42 amu, NCO^-, and (d) 26 amu, CN^-. The electron beam direction is longitudinal from bottom to top and the linear color scales represent ion counts in arbitrary units. (e) Ion kinetic energy for each channel in (a) - (d). Error bars represent one standard deviation of the statistical uncertainty.

the anion fragment. These observations are consistent with the recent work of Denifl and co-workers,[16,20] who determined that at these energies many of the DEA pathways for the uracil anion proceed via fast hydrogen-loss to a $[U - H]^-$ transient anion and subsequent decomposition over longer time scales to smaller anion and neutral fragments.

The measured H^- momentum distribution following DEA to uracil at 6.0 eV electron energy is displayed in Fig. 2(a). We find that H^- is preferentially ejected in the perpendicular or backwards directions with respect to the electron beam, with a sharp kinetic energy distribution that is displayed in Fig. 2(b). In order to better understand the partitioning between total translational kinetic energy release (KER) and internal energy of the fragments we have investigated the dependence of the KER on the incident electron energy. As the electron incident energy increases across the resonance, we see in Fig. 2(b) that the KER distribution becomes broader and the peak energy increases.

The minimum electron energy threshold for H^- production is 3.6 eV,[13,17,19,21] for H^- loss from the N1-H1 site as labeled by the inset schematic of Fig. 2(a), while the next-lowest

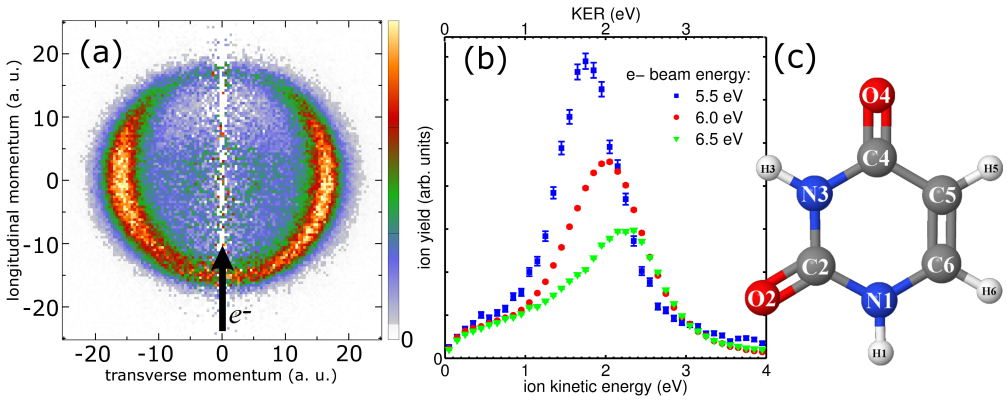

Figure 2: (a) Measured ion momentum distribution, in atomic units (a. u.), of H^- resulting from DEA to uracil at an electron beam energy of 6.0 eV. The electron beam direction is indicated by an arrow. Inset: the equilibrium geometry of uracil with site labels adopted in the text. (b) Kinetic energy distribution of H^- ions for the electron beam energies indicated, normalized for each electron incident energy to the cross section data of Ref. 13. Error bars indicate one standard deviation of the statistical uncertainty and the intensity scales are linear with arbitrary units.

threshold, from the C6-H6 site, is 4.2 eV.[13,17,19,21] The peak H^- kinetic energy increases from 1.8 eV to 2.3 eV, as the electron beam energy increases from 5.5 eV to 6.5 eV. These energetics strongly suggest that H^- originates from the N1-H1 site, confirming previous reports of two other groups.[14,15] Below 6.5 eV, the dissociation is likely to be primarily from that site, due to the absence of any significant additional structure in the 5.5 eV and 6.0 eV spectra. At 6.5 eV, we see an increase in ion yield at the low-energy shoulder appearing at H^- kinetic energies of about 1.5 eV, relative to the main peak at 2.2 eV. Due to conservation of momentum and the high relative mass of $[U - H]$, compared to H^-, the neutral fragment receives negligible translational kinetic energy from this two-body dissociation and the remaining energy is transferred to vibrational excitation of $[U - H]$, which manifests in the increasing width of the H^- kinetic energy peak of Fig. 2(b) with increasing electron energy.

Recent experimental and theoretical studies of DEA to polyatomic molecules have highlighted several examples[22–27] where fragment angular distributions can be predicted or reproduced on the basis of the axial recoil approximation.[28] Under such conditions the DEA product fragments are ejected along the axis connecting the centers-of-mass of the fragment

and the transient anion so that the fragment angular distribution is determined only by the electron attachment entrance amplitude,[29] which describes the probability for electron attachment as a function of the molecular orientation. DEA under axial recoil conditions efficiently channels the available energy into KER due to the strong repulsion of the anion potential energy surface along the reaction coordinate. Furthermore, in all of these examples the KER was observed to increase significantly as the electron energy was increased across the width of the resonance.[23–25] We observe such a trend in the KER for $[\mathrm{U} - \mathrm{H}] + \mathrm{H}^-$, as shown in the spectra of Figure 2(b). This correlation is a signature of the H^- fragment being rapidly ejected from the transient anion, with a relatively small dissipation of the residual energy E_r among the vibrational degrees of freedom within the molecular fragment. Here $E_r = E_e - (D_{(N1-H1)} - EA(H))$, where E_e is the incident electron energy, D is the bond dissociation energy and $EA(H) = 0.75$ eV[30] is the electron affinity of H.

To make a close comparison with experiment, we show as the continuous blue curve of Fig. 3 the result of averaging the square modulus of the calculated electron attachment entrance amplitude (see Supporting Information S2) over all relative orientations of the uracil molecule while holding fixed the angle between the electron direction $\overrightarrow{k}_{in}$ and the vector from N1 to H1, plotted as a function of that angle. The averaged square amplitude is shown as a polar plot, with the up direction corresponding to $\overrightarrow{k}_{in}$ and N1-H1 vector aligned and down corresponding to anti-aligned, so that, within the axial recoil approximation, these results may be compared directly to the measured H^- distribution plotted in the same figure (red circles). Although there are differences in detail, the experimental results for the angular distribution of H^- ions relative to the electron beam $\overrightarrow{k}_{in}$ show a similar trend to the theoretical prediction; in particular, the amplitude is large over a fairly wide range of angles centered on 90°, with angles greater than 90° moderately favored. The black dashed curve in Fig. 3 shows the distribution that results from the same body-frame entrance amplitude if we assume that H^- is produced by breaking the N3-H3 bond rather than the N1-H1 bond. In this case, the distribution is much less symmetric about 90°: backward angles are favored,

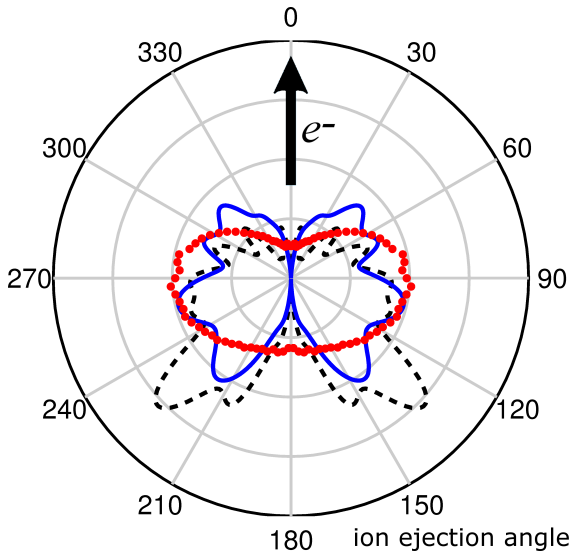

Figure 3: Polar plot of the measured (red circles) H^- anion fragment ion yield (radial coordinate) as a function of the ejection angle (angular coordinate); orientationally averaged square modulus of the entrance amplitude as a function of the angle θ between the electrons direction of incidence and the direction of the N1-H1 bond (continuous blue curve) and the N3-H3 bond (dashed black curve), with $\theta = 0°$ corresponding to the incident electron direction $\overrightarrow{k}_{in}$.

and there is a pronounced peak at about 140°. Overall agreement with the measured H^- distribution is much poorer.

These results support the conclusion reached above from energetic considerations that H^- is ejected from the N1 site and are in agreement with the experiments of Ptasińska *et al.*[14] and Almeida *et al.*[15] The broader features in the measured ion angular distribution that contrast with the angle-dependent structures of the axial recoil predictions could be due to the influence of the vibrationally excited states of the warm uracil target on the entrance amplitude, such as the broadening recently observed in DEA to methanol[9] or post-attachment dynamics in the anion that deviate subtly from axial recoil conditions.

At the resonant electron energy of 6.0 eV we measured the momentum distribution of $C_3H_3N_2O^-$ displayed in Fig. 4(a). The reaction channel leading to this fragment anion can be described by loss of H in conjunction with cleavage of either two C-N bonds or one C-N and one C-C bond. The ion kinetic energy distribution of Fig. 4(b) contrasts remarkably

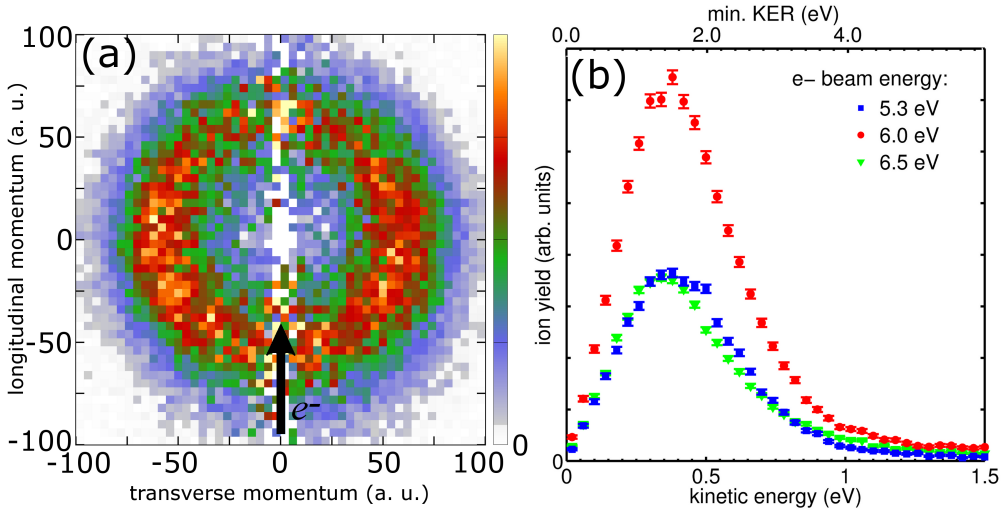

Figure 4: (a) As Fig. 2, for $C_3H_3N_2O^-$ at an electron beam energy of 6.0 eV. (b) As Fig. 2, kinetic energy and minimum KER distribution of $C_3H_3N_2O^-$ following DEA to uracil at the specified energies near 6.0 eV.

with those of Fig. 1(b), for the dissociation channels that likely proceed via unimolecular decomposition, suggesting an alternative dissociation mechanism. While the $C_3H_3N_2O^-$ kinetic energy is larger than the thermal-like kinetic energy distributions of Fig. 1(b), we observe no significant change in the ion kinetic energy for different electron beam energies within the width of the resonance, which indicates that the available excess energy above the dissociation threshold is channeled into vibrational excitation of the neutral fragment (either HCO or CO), or the anion fragment.

From the ion kinetic energy we derive the minimum KER, which is displayed on the upper horizontal axis of Fig. 4(b). This is the KER for the limiting case of a dissociation leading to a 2-body final state of HCO + $C_3H_3N_2O^-$, where the momentum is equally shared between the anion and one neutral fragment. In a generalized 3-body fragmentation we expect a larger KER, for the same measured anion kinetic energy, due to momentum sharing between the anion and two neutral fragments. In either case the bonds binding C2 or C4 within the ring must both break to release the neutral CO or HCO fragment with large kinetic energy compared to the vibrational excitation of either molecular fragment. In a slow unimolecular decay the uracil anion intermediate is likely to dissipate much of the available energy by

intramolecular vibrational redistribution.[31] Therefore we propose that this channel proceeds via a faster mechanism than the intermediate $[U - H]^-$ anion that is now understood[16,20] to be the common precursor to most of the alternative ring-breaking reaction pathways for electron energies above 4 eV.

In conclusion, the ion momentum distributions from DEA to uracil reported here show that two fragmentation channels occur via new pathways other than forming the metastable $[U - H]^-$ anion intermediate that was recently proposed as the dominant mechanism for DEA in nucleobases for electron energies above 4 eV. Based on our computational studies of the electornic structure and electron attachment dynamics (see Computational Methods and Supporting Information S2), we propose, as a possible candidate for this transient anion formed upon 6 eV electron attachment, a $^2A''$ Feshbach resonance. The kinetic energy spectrum of one fragment, $C_3H_3N_2O^-$, resulting from a ring-breaking dissociation, suggests surprisingly efficient channeling of the available electronic energy into KER rather than vibrational excitation.

Experimental methods

Using a dissociative electron attachment reaction microscope[32] (see Supporting Information S1 for details), we measured the 3-dimensional momentum distributions of anion fragments resulting from attachment of low-energy electrons to a molecular beam of pure uracil vapor. The electrons were produced in a pulsed beam with an energy distribution having a full width at half maximum of 0.8 eV using an electron gun. The target molecules were randomly orientated in the laboratory frame, therefore the direction of the anion momenta were measured relative to the electron beam direction.

Computational methods

The excited electronic states of uracil have been studied computationally by Epifanovsky and coworkers,[33] who identified a state of A'' symmetry (the 2 $^1A''$ state) at about 6 eV above the ground state. This state is described, in a one-electron picture, as resulting from the promotion of an electron from the highest π orbital, π_3, into a Rydberg-type σ orbital, σ_R, and is a plausible parent for a $(\pi_3)^1(\sigma_R)^2$ $^2A''$ Feshbach resonance near 6 eV that could account for the observed dissociative attachment in this energy region. In order to obtain an approximate description of such a Feshbach resonance, we first performed single-excitation configuration interaction (SECI) calculations on uracil using the electronic-structure package GAMESS[34] and the 6-31+G(d) basis set as contained therein. The 2 $^1A''$ state from this calculation fell at 6.85 eV and was, as expected, of $\pi_3 \rightarrow \sigma$ character. Our scattering calculations were carried out in the same 6-31+G(d) basis set as used for the electronic structure calculations, using the Schwinger multichannel (SMC) method. Details can be found in the Supporting Information S2.

Supporting Information Available

S1: Experimental details, S2: Computational details. This material is available free of charge via the Internet at `http://pubs.acs.org/`.

Acknowledgement

This work was supported by the Director, Office of Science, Office of Basic Energy Sciences, and by the Division of Chemical Sciences, Geosciences, and Biosciences of the U.S. Department of Energy under Contracts No. DE-AC02-05CH11231 (LBNL) and DE-FG02-97ER14814 (California Institute of Technology). The work of V.M. and C.W. made use of the Jet Propulsion Laboratory's Supercomputing and Visualization Facility. Y.A. acknowledges Japan Society for the Promotion of Science for support through Grants-in-Aid for

Scientific Research (No. 23600009).

References

(1) Sanche, L. In *Radiation damage in biomolecular systems*; García Gómez-Tejedor, G., Fuss, M. C., Eds.; Springer Netherlands: Dordrecht, 2012; pp 3–43.

(2) Uehara, S.; Nikjoo, H.; Goodhead, D. T. Comparison and assessment of electron cross sections for monte carlo track structure codes. *Rad. Res.* **1999**, *152*, 202.

(3) Cobut, V.; Frongillo, Y.; Patau, J.; Goulet, T.; Fraser, M.-J.; Jay-Gerin, J.-P. Monte Carlo simulation of fast electron and proton tracks in liquid water I. physical and physicochemical aspects. *Rad. Phys. and Chem.* **1998**, *51*, 229–243.

(4) Adaniya, H.; Rudek, B.; Osipov, T.; Haxton, D. J.; Weber, T.; Rescigno, T. N.; McCurdy, C. W.; Belkacem, A. Imaging the molecular dynamics of dissociative electron attachment to water. *Phys. Rev. Lett.* **2009**, *103*, 233201.

(5) Slaughter, D. S.; Adaniya, H.; Rescigno, T. N.; Haxton, D. J.; Orel, A. E.; McCurdy, C. W.; Belkacem, A. Dissociative electron attachment to carbon dioxide via the 8.2 eV Feshbach resonance. *J. Phys. B* **2011**, *44*, 205203.

(6) Ram, N. B.; Krishnakumar, E. Dissociative electron attachment resonances in ammonia: A velocity slice imaging based study. *J. Chem. Phys.* **2012**, *136*, 164308.

(7) Wu, B.; Xia, L.; Wang, Y.-F.; Li, H.-K.; Zeng, X.-J.; Tian, S. X. Renner-Teller effect on dissociative electron attachment to carbon dioxide. *Phys. Rev. A* **2012**, *85*, 052709.

(8) Szymańska, E.; Prabhudesai, V. S.; Mason, N. J.; Krishnakumar, E. Dissociative electron attachment to acetaldehyde, CH_3CHO. A laboratory study using the velocity map imaging technique. *Phys. Chem. Chem. Phys.* **2013**, *15*, 998.

(9) Slaughter, D. S.; Haxton, D. J.; Adaniya, H.; Weber, T.; Rescigno, T. N.; McCurdy, C. W.; Belkacem, A. Ion-momentum imaging of resonant dissociative-electron-attachment dynamics in methanol. *Phys. Rev. A* **2013**, *87*, 052711.

(10) Moradmand, A.; Slaughter, D. S.; Haxton, D. J.; Rescigno, T. N.; McCurdy, C. W.; Weber, T.; Matsika, S.; Landers, A. L.; Belkacem, A.; Fogle, M. Dissociative electron attachment to carbon dioxide via the $^2\Pi_u$ shape resonance. *Phys. Rev. A* **2013**, *88*, 032703.

(11) Ómarsson, F. H.; Szymanska, E.; Mason, N. J.; Krishnakumar, E.; Ingólfsson, O. Quantum superposition of target and product states in reactive electron scattering from CF_4 revealed through velocity slice imaging. *Phys. Rev. Lett.* **2013**, *111*.

(12) Feyer, V.; Plekan, O.; Richter, R.; Coreno, M.; Vall-llosera, G.; Prince, K. C.; Trofimov, A. B.; Zaytseva, I. L.; Moskovskaya, T. E.; Gromov, E. V. et al. Tautomerism in cytosine and uracil: An experimental and theoretical core level spectroscopic study. *J. of Phys. Chem. A* **2009**, *113*, 5736–5742.

(13) Denifl, S.; Ptasińska, S.; Hanel, G.; Gstir, B.; Probst, M.; Scheier, P.; Märk, T. D. Electron attachment to gas-phase uracil. *J. Chem. Phys.* **2004**, *120*, 6557.

(14) Ptasińska, S.; Denifl, S.; Grill, V.; Märk, T.; Illenberger, E.; Scheier, P. Bond- and site-selective loss of H^- from pyrimidine bases. *Phys. Rev. Lett.* **2005**, *95*, 093201.

(15) Almeida, D.; Ferreira da Silva, F.; Garca, G.; Limo-Vieira, P. Selective bond cleavage in potassium collisions with pyrimidine bases of DNA. *Phys. Rev. Lett.* **2013**, *110*, 023201.

(16) Ferreira da Silva, F.; Matias, C.; Almeida, D.; García, G.; Ingólfsson, O.; Flosadóttir, H. D.; Ómarsson, B.; Ptasińska, S.; Puschnigg, B.; Scheier, P. et al. NCO^-, a key fragment upon dissociative electron attachment and electron transfer to pyrimidine bases: Site selectivity for a slow decay process. *J. Am. Soc. Mass Spec.* **2013**, *24*, 1787–1797.

(17) González-Ramírez, I.; Segarra-Martí, J.; Serrano-Andrés, L.; Merchán, M.; Rubio, M.; Roca-Sanjuán, D. On the N_1-H and N_3-H bond dissociation in uracil by low energy electrons: A CASSCF/CASPT2 study. *J. Chem. Theory and Comput.* **2012**, *8*, 2769–2776.

(18) Bradforth, S. E.; Kim, E. H.; Arnold, D. W.; Neumark, D. M. Photoelectron spectroscopy of CN^-, NCO^-, and NCS^-. *J. Chem. Phys.* **1993**, *98*, 800.

(19) Li, X.; Sanche, L.; Sevilla, M. D. Low energy electron interactions with uracil: The energetics predicted by theory. *J. Phys. Chem. B* **2004**, *108*, 5472–5476.

(20) Denifl, S.; Zappa, F.; Mauracher, A.; Ferreira da Silva, F.; Bacher, A.; Echt, O.; Märk, T. D.; Bohme, D. K.; Scheier, P. Dissociative electron attachment to DNA bases near absolute zero temperature: Freezing dissociation intermediates. *ChemPhysChem* **2008**, *9*, 1387–1389.

(21) Hanel, G.; Gstir, B.; Denifl, S.; Scheier, P.; Probst, M.; Farizon, B.; Farizon, M.; Illenberger, E.; Märk, T. Electron attachment to uracil: Effective destruction at subexcitation energies. *Phys. Rev. Lett.* **2003**, *90*, 188104.

(22) Haxton, D. J.; McCurdy, C. W.; Rescigno, T. N. Angular dependence of dissociative electron attachment to polyatomic molecules: Application to the $^2B_1$ metastable state of the H_2O and H_2S anions. *Phys. Rev. A* **2006**, *73*, 062724.

(23) Adaniya, H.; Rudek, B.; Osipov, T.; Belkacem, A. Experimental study for dissociative electron attachment to water molecule in the $^2B_1$ resonance. *J. Phys.: Conf. Ser.* **2009**, *194*, 012031.

(24) Haxton, D. J.; Adaniya, H.; Slaughter, D. S.; Rudek, B.; Osipov, T.; Weber, T.; Rescigno, T. N.; McCurdy, C. W.; Belkacem, A. Observation of the dynamics leading to a conical intersection in dissociative electron attachment to water. *Phys. Rev. A* **2011**, *84*, 030701R.

(25) Ram, N. B.; Krishnakumar, E. Dissociative electron attachment to H_2S probed by ion momentum imaging. *Phys. Chem. Chem. Phys.* **2011**, *13*, 13621.

(26) Ómarsson, F. H.; Mason, N. J.; Krishnakumar, E.; Ingólfsson, O. State Selectivity and Dynamics in Dissociative Electron Attachment to CF_3I Revealed through Velocity Slice Imaging. *Angewandte Chemie International Edition* **2014**, *53*, 1–5.

(27) Ómarsson, F. H.; Ingólfsson, O.; Mason, N. J.; Krishnakumar, E. Dissociative electron attachment to CF3Cl: An experimental study using the velocity slice imaging technique. *Eur. Phys. J. D* **2012**, *66*.

(28) O'Malley, T.; Taylor, H. Angular dependence of scattering products in electron-molecule resonant excitation and in dissociative attachment. *Phys. Rev.* **1968**, *176*, 207–221.

(29) Haxton, D. J.; Zhang, Z.; Meyer, H.-D.; Rescigno, T. N.; McCurdy, C. W. Dynamics of dissociative attachment of electrons to water through the $^2B_1$ metastable state of the anion. *Phys. Rev. A* **2004**, *69*, 062714.

(30) Shiell, R. C.; Hu, X.; Hu, Q. J.; Hepburn, J. W. Threshold ion-pair production spectroscopy (TIPPS) of H_2 and D_2. *Farad. Discuss.* **2000**, *115*, 331–343.

(31) Nesbitt, D. J.; Field, R. W. Vibrational energy flow in highly excited molecules: Role of intramolecular vibrational redistribution. *J. Phys. Chem.* **1996**, *100*, 12735–12756.

(32) Adaniya, H.; Slaughter, D. S.; Osipov, T.; Weber, T.; Belkacem, A. A momentum imaging microscope for dissociative electron attachment. *Rev. Sci. Inst.* **2012**, *83*, 023106.

(33) Epifanovsky, E.; Kowalski, K.; Fan, P.-D.; Valiev, M.; Matsika, S.; Krylov, A. I. On the electronically excited states of uracil. *J. of Phys. Chem. A* **2008**, *112*, 9983–9992.

(34) Schmidt, M. W.; Baldridge, K. K.; Boatz, J. A.; Elbert, S. T.; Gordon, M. S.;

Jensen, J. H.; Koseki, S.; Matsunaga, N.; Nguyen, K. A.; Su, S. et al. General atomic and molecular electronic structure system. *J. Comput. Chem.* **1993**, *14*, 1347–1363.

DISCLAIMER

This document was prepared as an account of work sponsored by the United States Government. While this document is believed to contain correct information, neither the United States Government nor any agency thereof, nor the Regents of the University of California, nor any of their employees, makes any warranty, express or implied, or assumes any legal responsibility for the accuracy, completeness, or usefulness of any information, apparatus, product, or process disclosed, or represents that its use would not infringe privately owned rights. Reference herein to any specific commercial product, process, or service by its trade name, trademark, manufacturer, or otherwise, does not necessarily constitute or imply its endorsement, recommendation, or favoring by the United States Government or any agency thereof, or the Regents of the University of California. The views and opinions of authors expressed herein do not necessarily state or reflect those of the United States Government or any agency thereof or the Regents of the University of California.